Clays and Clay Minerals, Vol. 61, No. 4, 277–289, 2013.

A MULTI-TECHNIQUE CHARACTERIZATION OF CRONSTEDTITE SYNTHESIZED BY IRON–CLAY INTERACTION IN A STEP-BY-STEP COOLING PROCEDURE

I. Pignatelli[1,*], E. Mugnaioli[2], J. Hybler[3], R. Mosser-Ruck[1], M. Cathelineau[1], and N. Michau[4]

[1] GeoRessources UMR-CNRS 7359, Université de Lorraine, Faculté des sciences et technologies, Campus Aiguillettes, BP 70239, 54506 Vandœuvre-lès-Nancy, France
[2] Institut für Physikalische Chemie, Johannes Gutenberg-Universität Mainz, Welderweg 11, 55128 Mainz, Germany
[3] Institute of Physics, Academy of Science of Czech Republic, Cukrovarnicka 10, 16253 Prague 6, Czech Republic
[4] Agence nationale pour la gestion des déchets radioactifs (ANDRA), Direction Recherche et Développement/Service Colis et Matériaux, Parc de la Croix Blanche, 1/7 rue Jean Monnet, 92298 Châtenay-Malabry Cedex, France

Abstract—The cooling of steel containers in radioactive-waste storage was simulated in a step-by-step experiment from 90 to 40ºC. Among newly formed clay minerals observed in run products, cronstedtite was identified by a number of analytical techniques (powder X-ray diffraction, transmission electron microscopy, and scanning electron microscopy). Cronstedtite has not previously been recognized to be so abundant and so well crystallized in an iron−clay interaction experiment. The supersaturation of experimental solutions with respect to cronstedtite was due to the availability of Fe and Si in solution, as a result of the dissolution of iron metal powder, quartz, and minor amounts of other silicates. Cronstedtite crystals are characterized by various morphologies: pyramidal (truncated or not) with a triangular base and conical with a rounded or hexagonal cross-section. The pyramidal crystals occur more frequently and their polytypes ($2M_1$, $1M$, $3T$) were identified by selected area electron diffraction patterns and by automated diffraction tomography. Cronstedtite is stable within the 90−60ºC temperature range. At temperatures of $\leqslant$50ºC, the cronstedite crystals showed evidence of alteration.

Key Words—Cronstedtite, Experimental Iron–clay Interaction, MDO Polytypes, Radioactive Waste Storage.

INTRODUCTION

The present study presents a multi-technique characterization of cronstedtite crystals formed from an original experimental procedure on iron−clay interactions. The choice of this experiment was driven by the need to evaluate the effects of a progressive decrease in temperature expected during the cooling of nuclear-waste containers. Firstly, a mineralogical assemblage was obtained after heating at 90ºC an iron-clay mixture. The retrograde evolution was then simulated by a step-by-step cooling experiment between 90 and 40ºC. For the first time, single crystals of well crystallized cronstedtite were observed in run products and characterized accurately. The temperature-stability domain of cronstedtite was estimated on the basis of experimental evidence (occurrence and instability of crystals) and compared to literature data. Such detailed mineralogical characterization of the newly formed cronstedtite will be useful in improving databases of thermodynamic models.

* E-mail address of corresponding author:
isabella.pignatelli@univ-lorraine.fr
DOI: 10.1346/CCMN.2013.0610408

BACKGROUND

Cronstedtite is a T-O or 1:1 phyllosilicate, with a general formula $(Fe^{2+}_{3-x}Fe^{3+}_x)(Si_{2-x}Fe^{3+}_x)O_5(OH)_4$, with $0 < x < 0.8$ (Geiger *et al.*, 1983; Smrčok *et al.*, 1994; Hybler *et al.*, 2000, 2002; Kogure *et al.*, 2002), close to the initial ideal formula $(Fe^{2+}_2Fe^{3+})(SiFe^{3+})O_5(OH)_4$ proposed by Hendricks (1939). Chemical analyses of cronstedtite also show that the octahedrally coordinated iron can be replaced by other cations such as Mg^{2+}, Mn^{2+}, and Al^{3+} (Frondel, 1962; Geiger *et al.*, 1983) and that the tetrahedral sites can also contain Al^{3+} (Geiger *et al.*, 1983; Hybler *et al.*, 2002). Cronstedtite forms a solid solution with greenalite $(Fe^{2+},Fe^{3+},Mg,\square)_3(Si,Al)_2O_5(OH)_4$ (Guggenheim *et al.*, 1982), another Fe-rich layer silicate, from which it differs by the presence of ferric iron in tetrahedral coordination.

Like other trioctahedral T-O phyllosilicates, the standard polytypes of cronstedtite can be classified into four subfamilies, identical to Bailey's (1969) groups: A ($1M$, $2M_1$, $3T$ polytypes), B ($2O$, $2M_2$, $6H$), C ($1T$, $2T$, $3R$), and D ($2H_1$, $2H_2$, $6R$), on the basis of the interlayer shift and of the rotation between succeeding layers (Bailey, 1969). In the Order-Disorder theory (Dornberger-Schiff and Ďurovič, 1975), these polytypes are defined as MDO polytypes (Maximum Degree Order). Among them, only eight polytypes have been reported for cronstedtite in the literature (Table 1): $1T$, $1M$, $2H_1$, $2H_2$, $2M_1$, $2T$, $3T$, and $6R$ (Steadman and

https://doi.org/10.1346/CCMN.2013.0610408 Published online by Cambridge University Press

Table 1. Polytypes of trioctahedral T-O phyllosilicates and cronstedtite (literature data).

Polytypes of trioctahedral T-O phyllosilicates	MDO polytypes of trioctahedral T-O phyllosilicates				Authors
	A	B	C	D	Bailey (1969)
	1*M*, 2M_1, 3*T*	2*O*, 2M_2, 6*H*	1*T*, 2*T*, 3*R*	2H_1, 2H_2, 6*R*	
	MDO polytypes of cronstedtites				
	1*M*, 2M_1, 3*T*		1*T*, 2*T*	2H_1, 2H_2, 6*R*	Steadman and Nuttall, (1963, 1964)
Most frequent morphologies	Truncated trigonal pyramid shape, plates, needles (3*T*)		Cones or trigonally deformed cones (1*T*)	Ovoid-based shape or columnar with rounded hexagonal or circular cross section (group D). Ovoid-to barrel-shaped morphology (2H_2)	Frondel, (1962); Hybler *et al.* (2000; 2002); Steadman and Nuttall, (1963); Kogure *et al.*, (2001); Geiger *et al.* (1983)
Polytypes of trioctahedral T-O phyllosilicates	Non-MDO polytypes of cronstedtites: 9*R* Cornucopia mine (Nye Country, Nevada)				Frondel (1962)

Nuttall, 1963, 1964). One non-standard or non-MDO polytype was found by Frondel (1962) in a cronstedtite sample from the Cornucopia mine (Nye Country, Nevada, USA) and was given the Ramsdell symbol 9*R*.

In terrestrial environments, cronstedtite was found in sulfide veins as a low-temperature hydrothermal mineral, associated with siderite, pyrite, sphalerite, and quartz (Frondel, 1962) and also in metamorphosed massive sulfide deposits (López-García *et al.*, 1992). In Australian banded-iron formations of lower metamorphic grade, Gole (1980a, 1980b) reported the coexistence of greenalite with another mineral that he identified as probable cronstedtite. Cronstedtite also occurs in carbonaceous chondrites both in fine-grained rims and matrices as a product of aqueous alteration on the parent body (Müller *et al.*, 1979; Barber, 1981; Burbine and Burns, 1994; Browning *et al.*, 1996; Lauretta *et al.*, 2000; Zega and Buseck, 2003; Miyahara *et al.*, 2008).

A small number of experimental works reported the formation of T-O Fe-rich minerals of the serpentine group. Odinite $(R^{3+},R^{2+},\square)_3(Si_{2-x}Al_x)O_5(OH)_4$ and hexagonal crystals of cronstedtite as run products from the interaction of dioctahedral smectites with iron metal at 80ºC were reported by Lantenois (2003), Lantenois *et al.* (2005), and Lanson *et al.* (2012). Under similar experimental conditions, Fe-rich T-O phyllosilicates were described as "berthierine type" phases with the general formula $(R^{2+},R^{3+},\square)_3(Si_{2-x}, Al_x)O_5(OH)_4$ (Brindley, 1982) or "Fe-rich 7 Å clays" or "serpentine-like minerals" (Wilson *et al.*, 2006; Perronnet *et al.*, 2007; Mosser-Ruck *et al.*, 2010; Jodin-Caumon *et al.*, 2010, 2012; de Combarieu *et al.*, 2011; Rivard *et al.*, 2013), sometimes close to the greenalite end-member (Pierron, 2011). The numerous designations of low-temperature Fe-rich phyllosilicates found in the literature were explained by the difficulty in identifying the phases. They often appeared as highly disordered or nanocrystalline phases (Schlegel *et al.*, 2008), or as small crystals associated with Si-Al-Fe gels (Perronnet *et al.*, 2008), and can coexist with other Fe-rich phases in experimental run products.

MATERIALS AND METHODS

Starting material

The starting clay-rich rock used in the present experiments is a claystone from the Callovo-Oxfordian formation (denoted as COx) of the Paris Basin, a formation investigated for future waste storage in the underground research laboratory (URL) at the Meuse/Haute-Marne site of Bure (France). The claystone contains, on average, 41% clay minerals (illite and mixed-layer illite-smectite being the predominant clay minerals, and minor amounts of kaolinite and chlorite), 25% quartz, 31% carbonates (calcite and minor dolomite), and the remaining 3% consist of pyrite, phosphates, K-feldspar, and organic matter (Rousset, 2002; Gaucher *et al.*, 2004).

The starting products (experimental solutions and clays) were prepared under inert argon atmosphere using a solution of 0.0207 mol/kgw NaCl and 0.0038 mol/kgw $CaCl_2$ (pH = 6.4) and 1 g of claystone ground in a mortar to obtain a liquid/solid mass ratio of 10. Metal iron was added to the system as a powder (500 mg; average grain size ~40 μm) and as two plates with dimensions of nearly 3 mm × 6 mm × 1 mm (iron powder/COx mass ratio of 0.5). The starting mixture was divided into seven parts with each one placed into a Parr® non-stirred pressure vessel made of Teflon®, with a capacity of

https://doi.org/10.1346/CCMN.2013.0610408 Published online by Cambridge University Press

~20 mL. These vessels were heated in a furnace at 90(±2)ºC for 6 months and then the temperature was decreased every month in steps of 10ºC until it reached 40ºC. At each of the selected cooling temperatures, a vessel was removed from the oven. After quenching and opening of each vessel, the solid run products were dried under an argon flux at room temperature.

ManoCalcimeter

Quantitative analysis of carbonates was performed in the Museum National d'Histoire Naturelle (MNHN), Paris, using a Mélières manoCalcimeter (MCM) on 200 mg of bulk-rock sample powder (see Ledésert *et al.*, 2009). The MCM uses a 'Karbonat-Bombe' which is a simple apparatus consisting of a glass flask and a high-precision manometer (Dunn, 1980). The method gives a direct measurement of carbonates in rocks containing only calcite or aragonite ($CaCO_3$). The MCM is built to give a 100 mg value when 1 millimole of CO_2 is emitted during chemical attack on 100 mg (# 1 millimole) of $CaCO_3$ by 8 N hydrochloric acid. Nevertheless, the molecular weight of carbonates varying with their chemical composition and 100 mg of pure dolomite, for example, provokes the emission of 1.085 millimole of CO_2. As a consequence, the values read on the MCM must be corrected as a function of the amount of the different carbonates identified by X-ray diffraction (XRD). Calibration was performed using pure calcite crystals; the uncertainty precision was ~0.5 wt.%.

X-ray diffraction

The XRD data were collected at room temperature with a D8 Bruker diffractometer, using CoKα radiation (λ = 1.7902 Å), 35 kV accelerating voltage, and 45 mA beam intensity. The Bruker *DIFFRAC^{plus}* package was used for data acquisition and analysis.

The XRD patterns of randomly oriented powders were obtained using a scan step of 0.035º2θ and an exposure time of 3 s per step over a range of 3−54º2θ.

Scanning electron microscopy (SEM)

The secondary electron (SE) and backscattered electron (BSE) images of the cronstedtite crystals were obtained with an accelerating voltage of 15 kV using a cold-field emission gun (FEG) Hitachi S-4800. The lateral resolution of the FEG-SEM was ~1 nm for SE images. The crystals of cronstedtite analysed were collected on the iron plates, deposited on the carbon adhesive sticks, and then coated with carbon. Energy dispersive X-ray (EDX) spectra were recorded to identify the chemical elements present in the crystals.

Transmission electron microscopy (TEM) and EDX spectroscopy

The TEM images and EDX analyses were recorded at 200 kV using a Philips CM20 microscope with a point resolution of 0.27 nm equipped with Si-Li detector. The TEM specimens were prepared by dispersing the <2 μm fraction powders in ethanol under ultrasonic treatment and evaporating a drop of the suspension on a carbon network-like holey support film placed on a 200 mesh copper grid (Euromedex-Mundolcheim, France). The chemical composition of the run products was determined using EDX spectroscopy. The EDX spectra were recorded using a PGT spectrometer with an ultrathin window X-ray detector. The analyses were carried out in nanoprobe mode with a probe diameter of 10 nm using K_{AB} determined from clay standards with a similar thickness.

Selected area electron diffraction (SAED) patterns were recorded at 120 kV using a Philips CM120 microscope with a Digistar Nanomegas CCD camera.

Automated electron diffraction tomography (ADT)

3D electron diffraction data were also collected using a Tecnai F30 S-Twin microscope operating at 300 kV. Powdered sample (<2 μm fraction) was dispersed in ethanol, sonified, and sprayed onto a carbon-coated copper grid by a UIS250v Hielscher sonifier, according to the procedure described by Mugnaioli *et al.* (2009). Data collection was carried out by a combination of automated diffraction tomography (ADT) and precession electron diffraction (PED) (Kolb *et al.*, 2007, 2008; Mugnaioli *et al.*, 2009). Nano-electron diffraction patterns were collected in steps of 1º in a tilt range up to −60/+60º. Data processing, 3D reciprocal space reconstruction, and cell-parameter determination were performed using ADT3D software.

Analysis of solutions

The pH of each run solution was measured with a combination of a silver/sulfide electrode in a glove box after cooling at room temperature and 0.025 μm filtration. The electrode was calibrated using reference buffer solutions, certified by the Physikalisch-Technische Bundesanstalt (PTB, Germany) and the National Institute of Standards and Technology (NIST, USA), with pH 4, 7, and 10. The run solutions were diluted ten times in 2 vol.% HNO_3 and analyzed by inductively coupled plasma optical emission spectroscopy (ICP-OES) at LIMOS laboratory to determine the concentration of dissolved Si and Fe.

RESULTS

ManoCalcimeter and X-ray diffraction

The XRD patterns (Figure 1) of untreated mixed iron-COx sample and run samples revealed that the calcite reflection at 3.03 Å was unchanged in the 90 to 40ºC patterns, indicating that this mineral is unaffected by the cooling. As the manoCalcimeter results confirmed that the calcite content was constant (10±1 wt.%) in all samples, the XRD patterns were normalized to the calcite reflection (34.36º2θ). The intensities of quartz,

https://doi.org/10.1346/CCMN.2013.0610408 Published online by Cambridge University Press

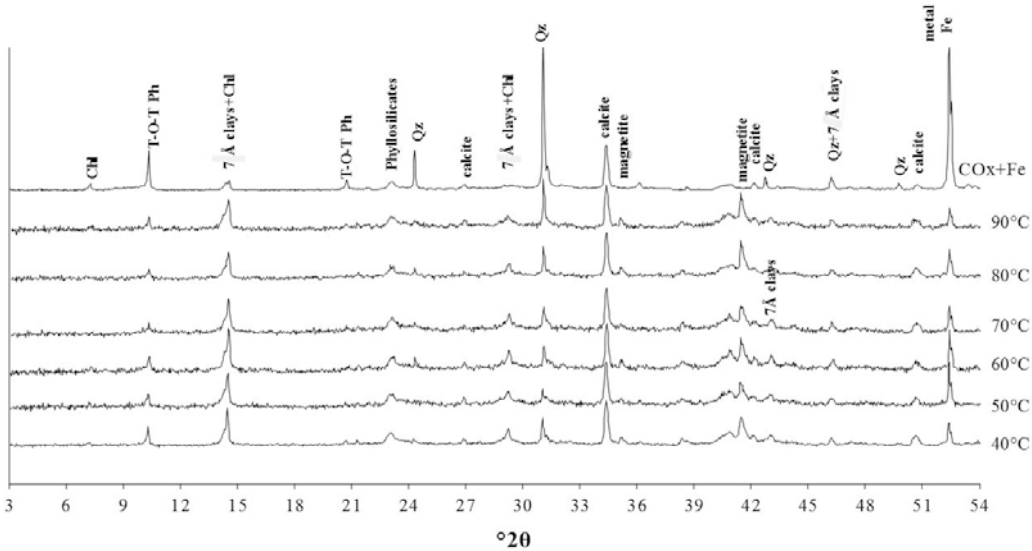


Figure 1. XRD patterns of samples collected from experiments run at 90 to 40ºC and of the untreated mixed iron-COx sample (Chl = chlorite, T-O-T Ph = T-O-T phyllosilicates, Qz = quartz).

iron metal, and T-O-T phyllosilicate (mica and illite) reflections decrease with decreasing temperature whereas the intensities of magnetite and 7 Å phyllosilicate reflections increase. This indicates a strong dissolution of quartz and iron metal (>70% for both phases) and partial destruction of T-O-T phyllosilicate layers. These XRD results highlight the increase in the amount of 7 Å clays in run products but fail to enable the accurate distinction of different T-O minerals because of their similar d_{hkl} values.

Scanning electron microscopy

The SEM analyses showed that the dominant 7 Å clays obtained in the 90ºC experiment were iron-rich and had different morphologies (Figure 2). Pyramidal (truncated or not) crystals with a triangular base and conical crystals were observed. The latter have rounded or hexagonal cross-sections (Figure 2a,b). The different morphologies coexisted down to temperatures of 70ºC (Figure 2c,d); at lower temperatures, the pyramidal morphology became dominant (Figure 2e,f).

Transmission electron microscopy

EDX analyses. The EDX analyses were performed on isolated particles of the <2 μm fraction powders. From the EDX results, structural formulae were calculated on the basis of seven oxygens, and the Fe^{3+}/Fe^{2+} ratio was adjusted to set the occupancy of the octahedral sites to 3. The compositions (expressed as a.p.f.u., *i.e.* atoms per formula unit) of 28 pyramidal crystals and five conical crystals formed at 90 and 80ºC are reported in Tables 2 and 3. The mean formula is:

$$(Fe^{2+}_{2.2}Fe^{3+}_{0.8})(Si_{1.2}Al_{0.1}Fe^{3+}_{0.7})O_5(OH)_4$$

The difference in the chemistry of the crystals with respect to their morphology is not significant considering the standard deviation (Tables 2, 3). The Si deficit and the presence of ferric iron in the tetrahedral sites are consistent with these two types of crystals both being cronstedtite.

TEM imaging. The TEM images showed that the greater crystallinity of the newly formed iron-rich clays was observed in the 70 and 60ºC run products (Figure 3) and also that this mineral became unstable at temperatures of ⩽50ºC, as demonstrated by alteration of its faces (Figure 4). At 40ºC, very rare relict crystals of altered cronstedtite were still observed.

SAED patterns and ADT/PED investigations: determination of cronstedtite polytypes

Because of their great abundance in the run product, pyramidal cronstedtites formed during the 70ºC experiment were chosen to identify their MDO polytypes following the procedure described by Ďurovič (1981). According to the Order-Disorder (OD) theory (Dornberger-Schiff, 1956, 1964, 1966, 1979), the superposition vectors and rotations (of almost identical 1:1 layers) needed to obtain the four possible subfamily structures are as follows: $\pm\mathbf{a}_i/3$ for subfamily A; $\pm\mathbf{b}/3$ or zero for subfamily C; and $\pm\mathbf{a}_i/3$ and $\pm\mathbf{b}/3$ or zero, combined with 180º rotation, for subfamilies B and D (Dornberger-Schiff, 1964; Bailey, 1969). The $\mathbf{a}_i$ and $\mathbf{b}$ are hexagonal and orthohexagonal unit-cell vectors, respectively.

It follows that the subfamily sublattice corresponding to the Fourier transform of subfamily structure is formed by reflections with $k = 3n$ (in orthohexagonal indexing, or $h–k = 3n$ in hexagonal indexing). These reflections are

https://doi.org/10.1346/CCMN.2013.0610408 Published online by Cambridge University Press

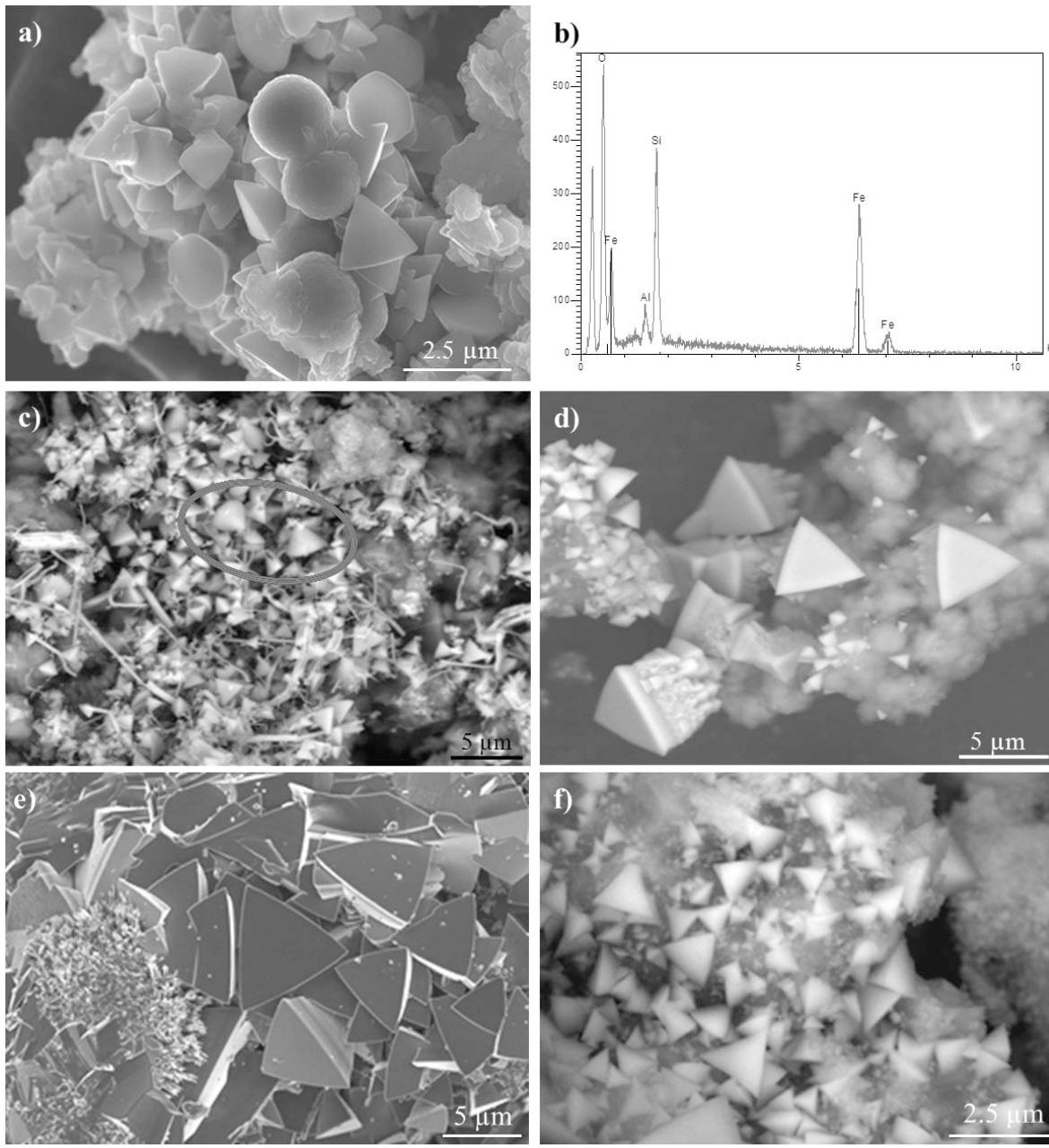


Figure 2. (a) SEM image of cronstedtite crystals with different morphologies in a 90ºC experiment and (b) the related EDX spectrum. (c,d) BSE images of conical (in circle) and pyramidal cronstedtites in a 70ºC experiment. (e,f) BSE and SE images of pyramidal crystals of cronstedtite in 60ºC experiments.

common to all polytypes belonging to the same subfamily and are consequently referred to as 'subfamily reflections.' Whereas the reflections having $k \neq 3n$ (in orthohexagonal indexing, or $h-k \neq 3n$ in hexagonal indexing) are typical of each polytype and are said to be 'non-family' or 'polytype reflections.' Diffraction patterns of two orthogonal reciprocal lattice sections are usually sufficient to identify an MDO polytype: the diffraction pattern of ($h0l$)* (hhl in hexagonal indexing) containing the subfamily reflections enabled the determination of the subfamily and the diffraction pattern from ($0kl$)*($\bar{h}hl$ in hexagonal indexing), containing both subfamily and polytype reflection useful in identifying the polytype (Ďurovič, 1997). In non-trigonal and non-hexagonal poytypes, however, the diffraction pattern of the ($0kl$)* plane is different from that of ($h0l$)*, because they are not symmetry equivalent (Ďurovič, pers. comm.). In order to determine such polytypes with

https://doi.org/10.1346/CCMN.2013.0610408 Published online by Cambridge University Press

Table 2. Cation contents (atom per formula unit, a.p.f.u.) in 28 pyramidal crystals of cronstedtite formed between 90 and 80ºC.

	Mg	Fe_{tot}	^{IV}Al	Si	^{IV}Fe	$^{VI}Fe^{2+}$	$^{VI}Fe^{3+}$
	0	3.79	0.02	1.19	0.79	2.18	0.81
	0.03	3.73	0.06	1.18	0.76	2.15	0.82
	0.02	3.68	0.09	1.20	0.70	2.18	0.80
	0	3.27	0.02	1.71	0.27	2.71	0.29
	0.10	3.54	0.19	1.17	0.64	2.07	0.83
	0.14	3.37	0.20	1.28	0.52	2.14	0.72
	0.03	3.71	0.11	1.15	0.74	2.12	0.88
	0.01	3.85	0.06	1.08	0.86	2.07	0.92
	0.01	3.73	0.04	1.22	0.74	2.21	0.78
	0.02	3.71	0.03	1.24	0.73	2.23	0.76
	0.01	3.81	0.02	1.16	0.82	2.15	0.84
	0	3.73	0.08	1.19	0.73	2.19	0.81
	0	3.89	0	1.11	0.89	2.11	0.89
	0.03	3.80	0.03	1.14	0.83	2.10	0.86
	0.07	3.35	0.27	1.31	0.42	2.24	0.70
	0	3.61	0.08	1.30	0.61	2.30	0.70
	0	3.84	0	1.16	0.84	2.16	0.84
	0.03	3.91	0.03	1.04	0.93	2.01	0.96
	0.06	3.59	0.10	1.25	0.65	2.19	0.75
	0	3.86	0	1.14	0.86	2.14	0.86
	0.04	3.89	0.03	1.04	0.93	2.00	0.96
	0.01	3.70	0.07	1.22	0.71	2.21	0.78
	0.02	3.82	0.07	1.10	0.84	2.08	0.90
	0.01	3.71	0.06	1.22	0.72	2.21	0.78
	0	3.77	0	1.23	0.77	2.23	0.77
	0	3.88	0	1.12	0.88	2.12	0.88
	0.01	3.76	0.05	1.18	0.77	2.18	0.82
	0.01	3.81	0.09	1.10	0.81	2.09	0.90
	0.06	3.27	0.28	1.38	0.33	2.32	0.61
Average	0.03	3.70	0.07	1.20	0.73	2.17	0.80
σ	0.03	0.18	0.08	0.13	0.16	0.13	0.13

certainty, the (0*kl*)* planes should be recorded and checked also.

The distribution of spots on experimental electron diffraction 2D patterns were compared with the identification diagrams for MDO polytypes of cronstedtite described in the literature (Ďurovič, 1997; Hybler *et al.*, 2008), and with diffraction patterns calculated theoretically with the aid of the *DIFK91* program (Smrčok and Weiss, 1993).

The SAED patterns of several pyramidal cronstedtites indicated that they are all 1*M* polytypes. The spot distribution along the 11*l* reciprocal lattice row on the (hhl_{hex})* plane indicates that these crystals belong to subfamily A (Bailey's group) (Figure 5). Moreover, the spot distribution on $(h0l_{hex})$* and $(0kl_{hex})$* planes corresponds to MDO groups II and I, respectively (Figure 6). Both are in agreement with theoretically calculated patterns. The 1*M* cronstedtite polytype is very rare and generally occurs intergrown with the 3*T* polytype and is strongly disordered (Ďurovič, 1997).

Three ADT data sets were collected on different crystals and reconstructed in 3D diffraction volumes.

Table 3. Cation contents (a.p.f.u) in five conical crystals of cronstedtite formed between 90 and 80ºC.

	Mg	Fe_{tot}	^{IV}Al	Si	^{IV}Fe	$^{VI}Fe^{2+}$	$^{VI}Fe^{3+}$
	0.01	3.74	0.07	1.18	0.75	2.17	0.82
	0.04	3.60	0.14	1.22	0.64	2.18	0.78
	0.04	3.59	0.15	1.21	0.63	2.17	0.79
	0.01	3.75	0.10	1.14	0.76	2.13	0.86
	0.04	3.53	0.26	1.17	0.58	2.12	0.84
Average	0.03	3.64	0.14	1.18	0.67	2.16	0.82
σ	0.02	0.10	0.07	0.03	0.08	0.03	0.03

https://doi.org/10.1346/CCMN.2013.0610408 Published online by Cambridge University Press

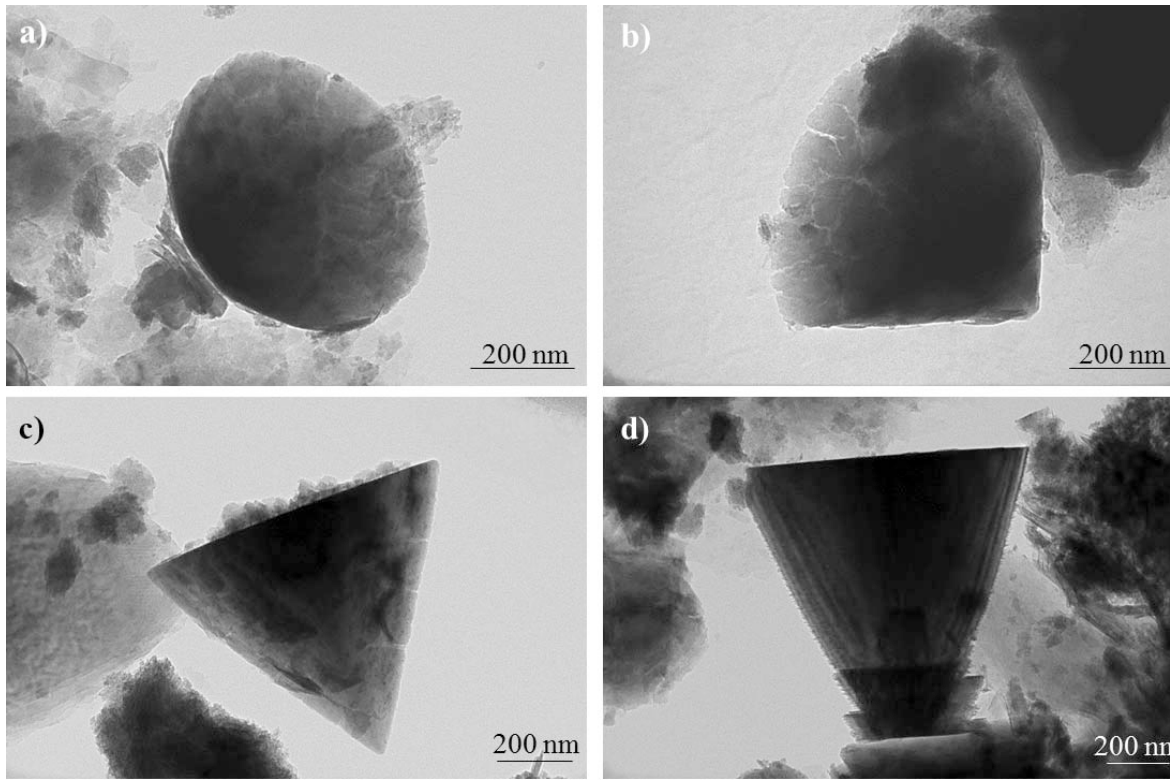


Figure 3. TEM images of conical (a,b) and pyramidal cronstedtites (c,d) formed between 90 and 80ºC.

The first acquisition, from a well shaped pyramidal crystal (Figure 7a), showed diffuse scattering along c^* for both $h0l_{hex}$ and hhl_{hex} reflections, so that no polytypic identification could be made (Figure 7b).

The second acquisition was from a pyramidal crystal, where two corners were truncated and one not (Figure 8a). Remarkably the corner not truncated was characterized by diffuse disorder, while the rest of the crystal delivered a mostly coherent diffraction consistent with the subfamily A and with MDO group III, *i.e.* the $2M_1$ polytype (Figure 8b–d). The cell is *C*-centered monoclinic with parameters a = 5.5 Å, b = 9.6 Å, c = 14.4 Å, β = 97.4º. Systematic absences of reflections $h0l$ with $l \neq 2n$ suggested the presence of a glide plane c perpendicular to the b axis. This is in agreement with the

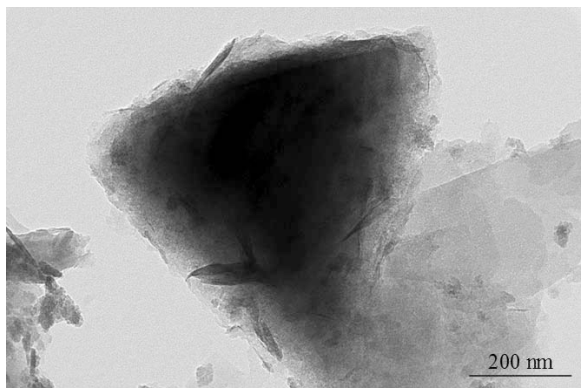


Figure 4. TEM image of unstable cronstedtite crystal in a 50ºC experiment.

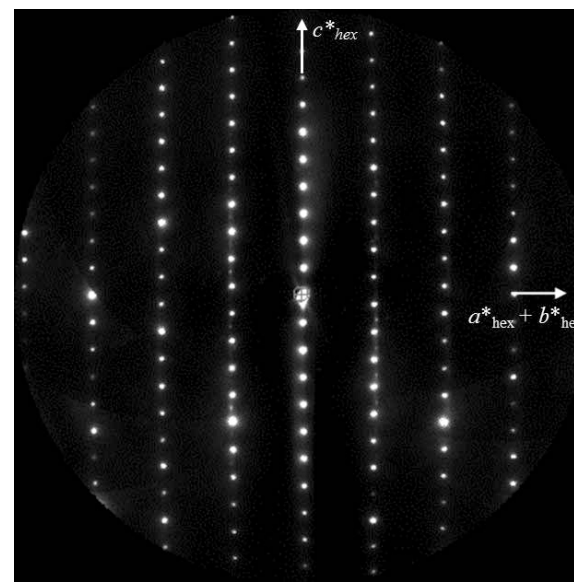


Figure 5. SAED pattern of a $(hhl_{hex})^*$ plane for the 1*M* polytype of cronstedtite. Note that the pattern also contains a few weak parasitic spots of an unidentified phase.

https://doi.org/10.1346/CCMN.2013.0610408 Published online by Cambridge University Press

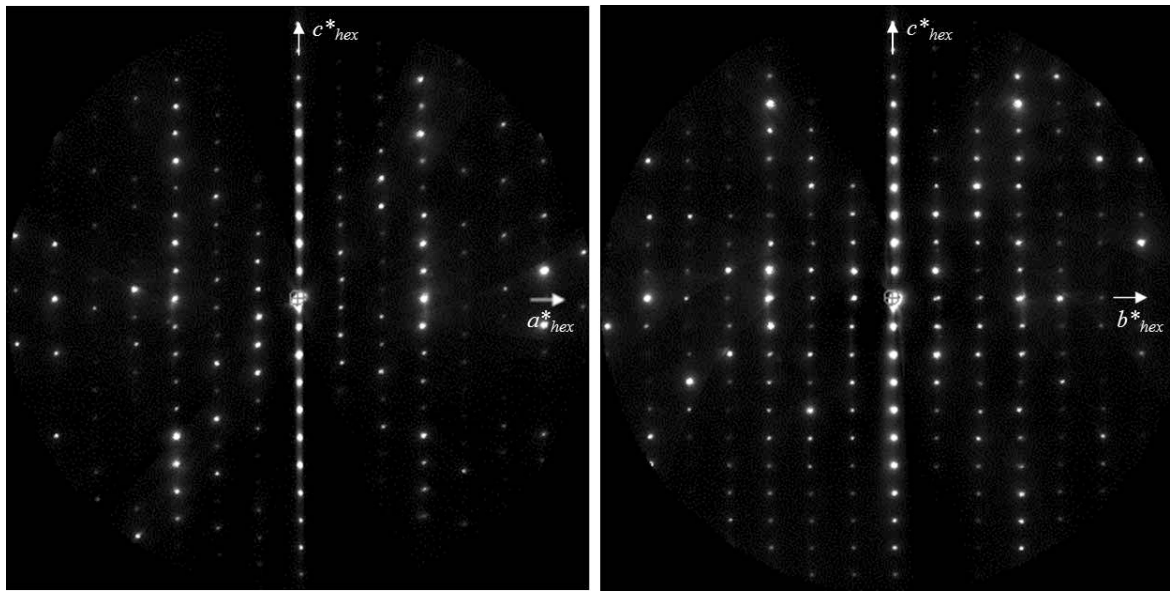


Figure 6. SAED patterns of the $(h0l_{hex})^*$ (left) and $(0kl_{hex})^*$ (right) planes for 1*M* polytype.

space group *Cc* found by Steadman and Nuttall (1964) for this polytype. Worth noting is that the $2M_1$ polytype of cronstedtite is also very rare in nature (Ďurovič, 1997). The presence of diffuse scattering along *c** further testifies to a certain degree of disorder even in the most ordered parts of the crystal.

The third acquisition highlighted the presence of another polytype belonging to subfamily A and MDO group IV, *i.e.* 3*T* polytype (Figure 9a–b). The cell is hexagonal with parameters $a = 5.5$ Å and $c = 21.4$ Å. The intensity distribution suggests a trigonal symmetry (Laue class $P\bar{3}$ or $P\bar{3}1m$), consistent with the space group $P3_1$ reported in the literature (Steadman and Nuttall, 1963; Smrčok *et al.*, 1994).

Solution chemistry

The characterization of the run solutions showed that the mean pH value was 7.47±0.16 and that the Si

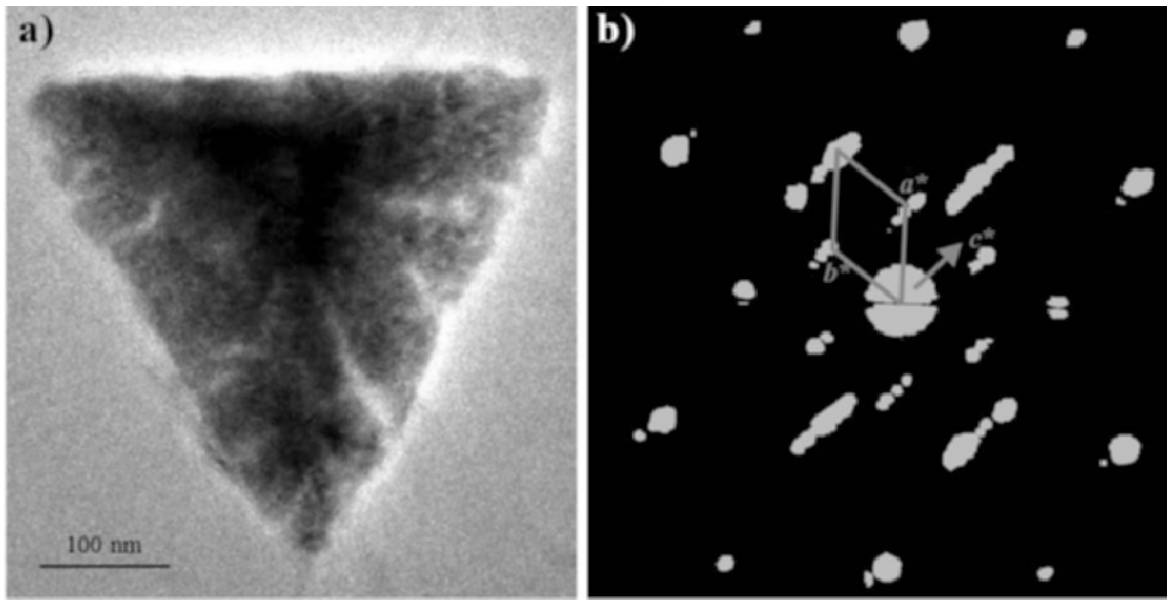


Figure 7. First ADT acquisition: (a) TEM image of the pyramidal crystal selected for ADT acquisition; (b) ADT 3D diffraction reconstruction (along an oblique view) showing the diffuse scattering along *c**.

https://doi.org/10.1346/CCMN.2013.0610408 Published online by Cambridge University Press

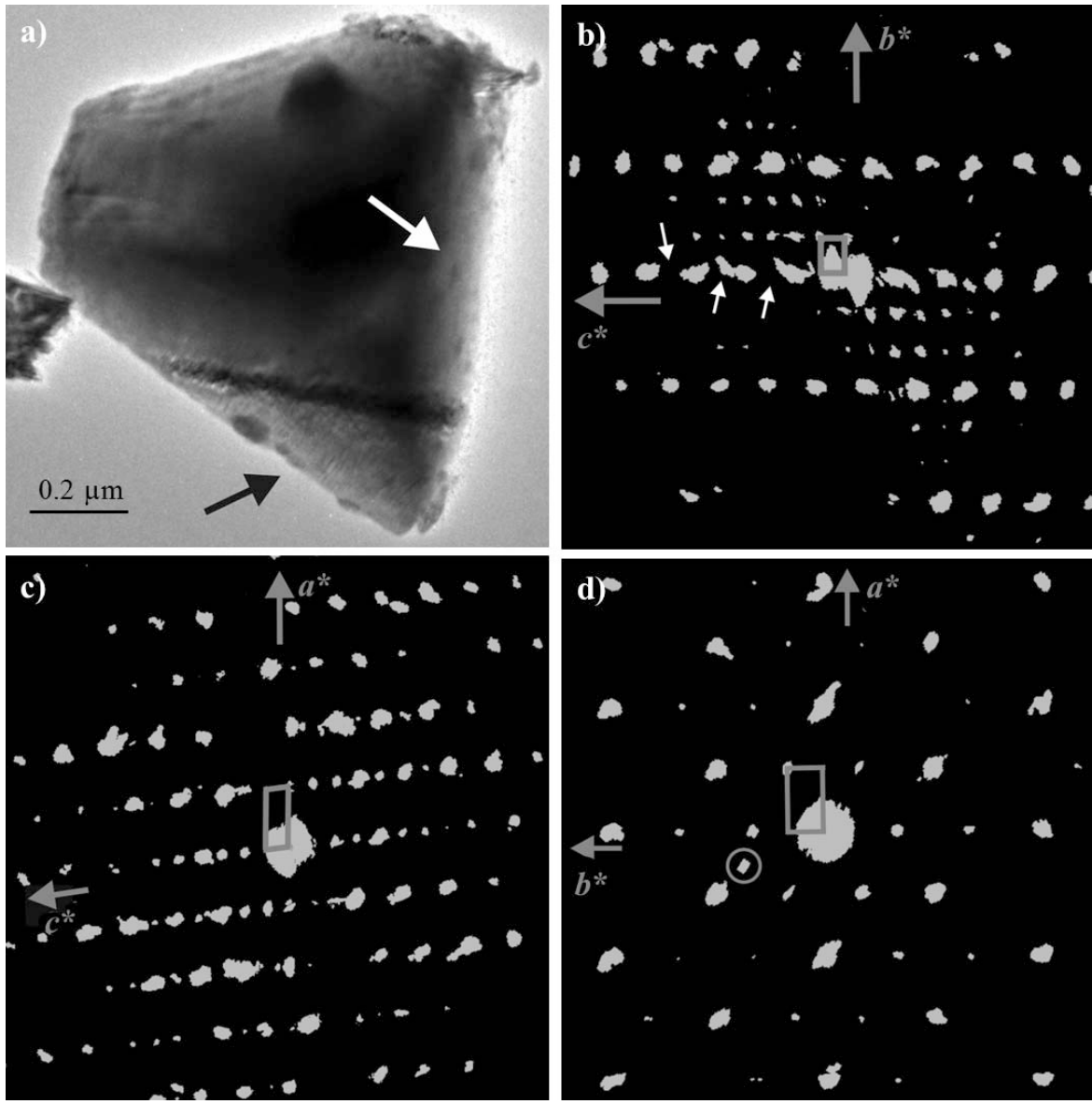


Figure 8. Second ADT acquisition: (a) TEM image of the truncated crystal. The area indicated by the black arrow was affected by diffuse disorder, while the area indicated by the white arrow was selected for ADT acquisition. (b) ADT 3D diffraction reconstruction viewed along a^*. White arrows indicate the reflections $h0l$ with $l \neq 2n$ extinct due to the c-glide plane. (c) ADT 3D diffraction reconstruction viewed along b^*. (d) ADT 3D diffraction reconstruction viewed along c^*. An extraneous reflection from another crystal is marked with a circle. Note that these are projections of a 3D diffraction volume and not conventional 2D electron diffraction patterns.

concentration varied between 7 and 11 ppm as a function of the temperature in the experiments (Figure 10). The quartz solubility at each run temperature was calculated using the *PHREEQC* geochemical software package V2.17 (Parkhurst and Appelo, 1999) and the associated LLNL database (Johnson *et al.*, 2000). The Si concentration was under the quartz solubility curve in the run solution of experiments carried out in the temperature range of 90−60ºC, whereas at 50ºC the Si concentration was on the quartz solubility curve. Finally, the Si concentration increased slightly in the last run solution (40ºC). The Fe concentration in the experimental solutions was very low (<1 ppm) or below the detection limit.

DISCUSSION AND CONCLUSIONS

The significant decrease in the intensity of the quartz, T-O-T phyllosilicates, and iron metal XRD reflections indicates that these phases were dissolved, releasing Si

https://doi.org/10.1346/CCMN.2013.0610408 Published online by Cambridge University Press

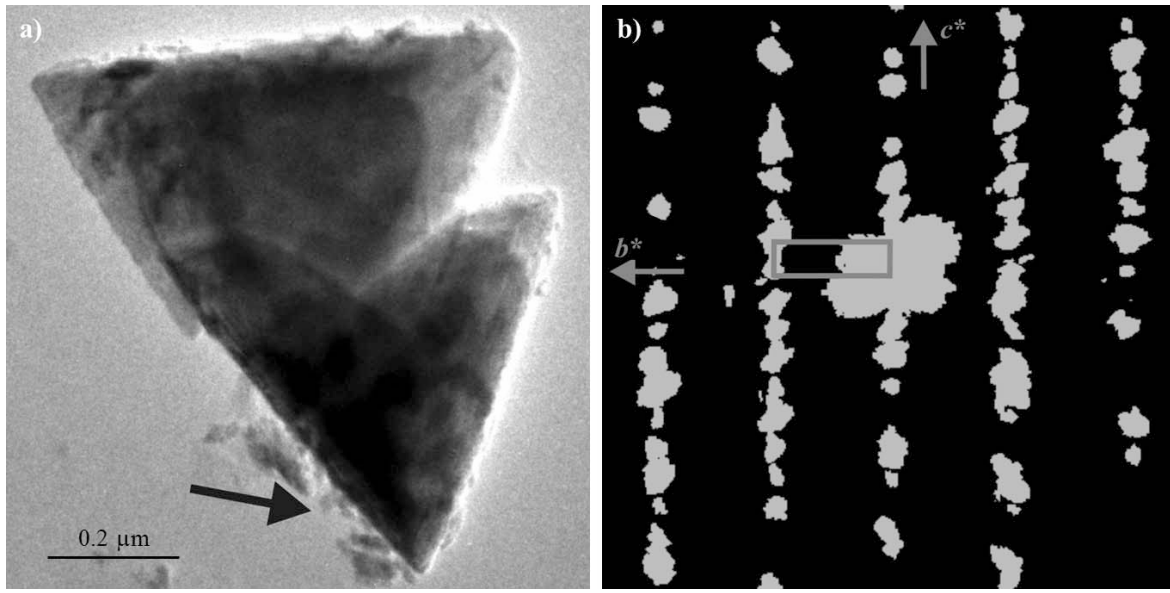


Figure 9. Third ADT acquisition: (a) TEM image of the crystal selected for the acquisition (indicated by a black arrow); (b) ADT 3D diffraction reconstruction viewed along *a** showing the 21.4 Å periodicity.

and Fe into the experimental solutions. The dissolution of quartz was confirmed by the Si concentration, measured in the run solutions, which was less than that at equilibrium with quartz between 90 and 60ºC (Figure 10). Over that temperature range, cronstedtite was formed together with other 7 Å clay minerals. As the iron content in the run solutions was <1 ppm or below the detection limit (<5 ppb), all of the iron must have been incorporated into the newly formed minerals (cronstedtite, magnetite, and other Fe-rich silicates). At temperatures of 50 and 40ºC, the Si content measured was equal to or greater than that at equilibrium with quartz, preventing the precipitation of cronstedtite. Using the step-by-step cooling procedure presented here, the stability range of cronstedtite with respect to temperature was established. Between 90 and 60ºC, cronstedtite appeared to be stable; 50ºC was the lower limit of cronstedtite stability, as confirmed by crystal alteration (see the results section). The upper limit was $\geqslant$90ºC but cannot be determined accurately. No cronstedtite was observed in similar experiments carried out on the same claystone (COx) at the higher temperatures of 150 and 300ºC (Pierron, 2011).

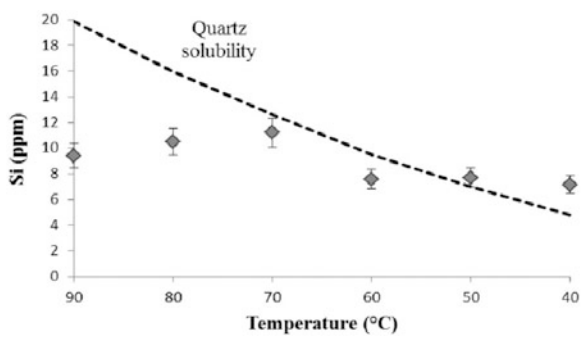


Figure 10. Si concentration (ppm) in run solutions *vs.* experimental temperature.

The cooling experiments from 90 to 60ºC favored the development of crystals with pyramidal (truncated or not) morphologies and enhanced crystallinity. Pyramidal crystals analyzed by TEM showed different polytypic sequences and various degrees of disorder. The polytypes identified, all belonging to the subfamily A, are $2M_1$ and 1*M* together with 3*T*. According to Hybler *et al.* (2008), these two monoclinic polytypes are very rare whereas the 3*T* polytype is relatively abundant in nature. The mean formula for pyramidal polytypes is in good agreement with that reported by Kogure *et al.* (2002) for cronstedtite of subfamily A, even if the crystals in the present study contain small amounts of Al and Mg (Table 2). Conical crystals of cronstedtite co-occurred with pyramidal crystals only in the 90 and 80ºC experiments. The coexistence of these two different morphologies may be due to changes in the degree of supersaturation during growth. When the supersaturation decreased, the crystals took on a polyhedral habit bounded by flat faces (Sunagawa, 2005), changing the morphology from conical to pyramidal. In accordance with the literature, the conical crystals may well be cronstedtite polytypes belonging to the C or D subfamilies (Frondel, 1962; Kogure *et al.*, 2001; Hybler *et al.*, 2002). The co-occurrence of one of these two subfamilies with the subfamily A was observed (C + A or D + A subfamilies) by Hybler *et al.* (2008). A detailed study of the conical crystals is currently under development and will be the subject of a future publication.

https://doi.org/10.1346/CCMN.2013.0610408 Published online by Cambridge University Press

Comparison with cronstedtite from chondrites

Several studies of the formation conditions of cronstedtite were carried out on carbonaceous chondrites in which this mineral is the dominant component (Dyl *et al.*, 2010). Cronstedtite crystals in meteorites are often small and platy, and characterized by high degrees of stacking disorder (Müller *et al.*, 1979; Lauretta *et al.*, 2000; Zega and Buseck, 2003), making the identification of their polytypes difficult. Nevertheless, Müller *et al.* (1979) and Zega and Buseck (2003) found mostly 1*T* polytype; Müller *et al.* (1979) reported that the second, more frequent polytype is 1*M*. Even if the conditions of cronstedtite formation in meteorites are close to those of the present experiments (presence of metallic Fe, neutral-alkaline solution, reducing conditions), the 1*T* polytype was not observed in the run products of the present experiments. Mass-transfer and reaction-path calculations simulating aqueous alteration in chondrites suggest that the upper limit of cronstedtite stability is 90−100ºC (Schulte and Shock, 2004; McAlister and Kettler, 2008). These calculations were carried under the hypothesis that the activity of silica in solution is close to quartz saturation; the chemical data obtained from the present experimental solutions disagree and indicate that the aqueous silica activity is below the level of quartz saturation between 90 and 70ºC.

Comparison with run products in similar experimental conditions

The results presented indicate that the occurrence of cronstedtite is restricted to the 90−50ºC temperature domain. At 90ºC, in the 6 months experiment, cronstedtite was not as abundant and its degree of crystallinity was low. Is this a kinetic or temperature effect? To answer this question, the results were compared with those of similar experiments carried out on the same starting materials. Rivard (2011) and Pierron (2011) used the same claystone (COx of the Meuse/Haute-Marne site of Bure) at 90ºC for 9 months but employed slightly different liquid/solid mass ratios (20 and 10, respectively) and iron powder/COx mass ratios (0.2 and 0.1 or 1, respectively). Those authors observed the crystallization of iron-rich T-O clays with a composition between those of odinite, berthierine, and greenalite (Figure 11). No cronstedtite was reported by those authors. The results seem to confirm that the formation of cronstedtite is strongly favored by a lower temperature range, and maybe by a temperature decrease.

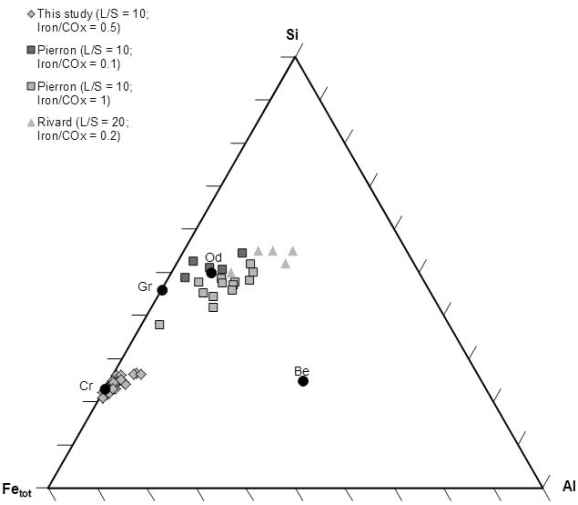


Figure 11. Chemical composition of the most evolved newly formed T-O clays plotted in a Si-Al-Fe_{tot} ternary diagram. Values obtained from the present study are represented by diamonds. The experiments of Pierron (2011) and Rivard (2011) are represented by squares and triangles, respectively. Gr: greenalite $(Fe^{3+}_{0.45}Fe^{2+}_{1.9}Mg_{0.3}\square_{0.35})Si_{2.0}O_5(OH)_4$ (Guggenheim *et al.*, 1982); Od: odinite $(Al_{0.15}Fe^{3+}_{1.2}Fe^{2+}_{0.35}Mg_{0.7}\square_{0.6})(Si_{1.85}Al_{0.15})O_5(OH)_4$ (Bailey, 1988); Be: berthierine $(Al_{0.96}Fe^{3+}_{0.22}Fe^{2+}_{1.49}Mg_{0.17}\square_{0.17})(Si_{1.15}Al_{0.85})O_5(OH)_4$ (Brindley, 1982); Cr: cronstedtite $(Fe^{3+}_{0.84}Fe^{2+}_{2.16})(Si_{1.16}Fe^{3+}_{0.84})O_5(OH)_4$ (Kogure *et al.*, 2002).

CONCLUSIONS

In clay formations which may host deep geological radioactive waste disposal, a first increase in temperature to 90ºC close to the containers followed by cooling is expected. The present experiments simulated the mineralogical evolution of the iron-clay system around the steel containers during cooling between 90 and 40ºC. They showed that the composition of Fe-rich T-O clays stable at 90ºC (close to odinite, greenalite, or berthierine) will evolve toward cronstedtite during cooling. This result has to be taken into account in the understanding of complex interaction in glass-iron-clay systems.

ACKNOWLEDGMENTS

The authors thank L. Mouton and J. Ghanbaja for SEM and TEM images and analyses at SCMEM laboratory (Université de Lorraine, France). U. Kolb is thanked warmly for providing access to the TEM laboratory at the Institut für Physikalische Chemie, Johannes Gutenberg Universität. The authors also thank M. Klementova and L. Palatinus for collecting and processing the SAED patterns and L. Truche for helpful discussion. This research was supported financially by ANDRA – Agence Nationale pour la gestion des Déchets Radioactifs (French national agency for the management of radioactive wastes).

REFERENCES

Bailey, S.W. (1969) Polytypism of trioctahedral 1:1 layer silicates. *Clays and Clay Minerals*, **17**, 355−371.

Bailey, S.W. (1988) Odinite, a new dioctahedral-trioctahedral Fe^{3+}-rich 1:1 clay mineral. *Clay Minerals*, **23**, 237−247.

Barber, D.J. (1981) Matrix phyllosilicates and associated minerals in C2M carbonaceous chondrites. *Geochimica et Cosmochimica Acta*, **45**, 945−970.

Brindley, G.W. (1982) Chemical compositions of berthierines – A review. *Clays and Clay Minerals*, **30**, 153−155.

Browning, L.B., McSween, H.Y. Jr., and Zolensky, M.E. (1996) Correlated alteration effects in CM carbonaceous

https://doi.org/10.1346/CCMN.2013.0610408 Published online by Cambridge University Press

chondrites. *Geochimica et Cosmochimica Acta*, **60**, 2621–2633.

Burbine, T.H. and Burns, R.G. (1994) Questions concerning the oxidation of the ferrous iron in carbonaceous chondrites. *Lunar Planetary Science*, **XXV**, 199–200.

de Combarieu, G., Schlegel, M.L., Neff, D., Foy, E., Vantelon, D., Barboux, P., and Gin, S. (2011) Glass-iron-clay interactions in a radioactive waste geological disposal: an integrated laboratory-scale experiment. *Applied Geochemistry*, **26**, 65–79.

Dornberger-Schiff, K. (1956) On Order-Disorder Structures (OD-Structures). *Acta Crystallographica*, **9**, 593–601.

Dornberger-Schiff, K. (1964) Grundzüge einer Theorie von OD-Strukturen aus Schichten. Abh. dtsch. Akad Wiss Berlin, Kl. f. Chem., **3**, 107 pp.

Dornberger-Schiff, K. (1966) Lehrgang üer OD-Strukturen. Akademine-Verlag, Berlin, 135 pp.

Dornberger-Schiff, K. and Ďurovič, S. (1975) OD-interpretation of kaolinite-type structure – I: symmetry of kaolinite packets and their stacking possibilities. *Clays and Clay Minerals*, **23**, 219–229.

Dornberger-Schiff, K. (1979) OD structures – a game and a bit more. *Kristall Und Technik*, **14**, 1027–1045.

Dunn, D.A. (1980) Revised techniques for quantitative calcium carbonate analysis using the "Karbonat-Bombe," and comparisons to other quantitative carbonate analysis methods. *Journal of Sedimentary Research*, **50**, 631–636.

Ďurovič, S. (1981) OD-Charakter, Polytypie und Identifikation von Schichtsilikaten. *Fortschritte der Mineralogie*, **59**, 191–226.

Ďurovič, S. (1997) Cronstedtite-1*M* and co-existence of 1*M* and 3*T* polytypes. *Ceramics – Silikáty*, **41**, 98–104.

Dyl, K.A., Manning, C.E., and Young, E.D. (2010) The implication of the cronstedite in water-rich planetesimals and asteroids. Astrobiology Science Conference 2010, League City, Texas, USA.

Frondel, C. (1962) Polytypism in cronstedtite. *American Mineralogist*, **47**, 781–783.

Gaucher, E., Robelin, C., Matray, J.M., Négrel, G., Gros, Y., Heitz, J.F., Vinsot, A., Rebours, H., Cassagnabère, A., and Bouchet, A. (2004) ANDRA underground research laboratory: interpretation of the mineralogical and geochemical data acquired in the Callovian-Oxfordian formation by investigative drilling. *Physics and Chemistry of the Earth*, **29**, 55–77.

Geiger, C.A., Henry, D.L., Bailey, S.W., and Maj, J.J. (1983) Crystal structure of cronstedtite-2H_2. *Clays and Clay Minerals*, **31**, 97–108.

Gole, M.J. (1980a) Low-temperature retrograde minerals in metamorphosed Archean banded iron-formations, Western Australia. *The Canadian Mineralogist*, **18**, 205–214.

Gole, M.J. (1980b) Mineralogy and petrology of very-low metamorphic grade Archean banded iron-formations, Weld Range, Western Australia. *American Mineralogist*, **65**, 8–25.

Guggenheim, S., Bailey, S.W., Eggleton, R.A., and Wilkes, P. (1982) Structural aspects of greenalite and related minerals. *The Canadian Mineralogist*, **20**, 1–18.

Hendricks, S.B. (1939) Random structures of layer minerals as illustrated by cronstedtite ($2FeO{\cdot}Fe_2O_3{\cdot}SiO_2{\cdot}2H_2O$). Possible iron content of kaolin. *American Mineralogist*, **24**, 529–539.

Hybler, J., Petříček, V., Ďurovič, S., and Smrčok, L. (2000) Refinement of the crystal structure of cronstedtite-1*T*. *Clays and Clay Minerals*, **48**, 331–338.

Hybler, J., Petříček, V., Fábry, J., and Ďurovič, S. (2002) Refinement of the crystal structure of cronstedtite-2H_2. *Clays and Clay Minerals*, **50**, 601–613.

Hybler, J., Ďurovič, S., and Kogure, T. (2008) Polytypism in cronstedtite. *Acta Crystallographica*, **A64**, C498–499.

Jodin-Caumon, M.C., Mosser-Ruck, R., Rousset, D., Randi, A., Cathelineau, M., and Michau, N. (2010) Effect of a thermal gradient on iron–clay interactions. *Clays and Clay Minerals*, **58**, 667–681.

Jodin-Caumon, M.C., Mosser-Ruck, R., Randi, A., Pierron, O., Cathelineau, M., and Michau, N. (2012) Mineralogical evolutions of a claystone after reaction with iron under thermal gradient. *Clays and Clay Minerals*, **60**, 5, 443–455.

Johnson, L., Anderson, G., and Parkhurst, D. (2000) Database from '*thermo.com.V8.R6.230*' Prepared at Lawrence Livermore National Laboratory, California, USA (Revision: 1.11).

Kogure, T., Hybler, J., and Ďurovič, S. (2001) A HRTEM study of cronstedtite: determination of polytypes and layer polarity in trioctahedral 1:1 phyllosilicates. *Clays and Clay Minerals*, **49**, 310–317.

Kogure, T., Hybler, J., and Yoshida, H. (2002) Coexistence of two polytypic groups in cronstedtite from Lostwithiel England. *Clays and Clay Minerals*, **50**, 504–513.

Kolb, U., Gorelik, T., Kübel, C., and Otten, M.T. (2007) Towards automated diffraction tomography: Part I – Data acquisition. *Ultramiscoscopy*, **107**, 507–513.

Kolb, U., Gorelik, T., and Otten, M.T. (2008) Towards automated diffraction tomography. Part II – Cell parameter determination. *Ultramicroscopy*, **108**, 763–772.

Lanson, B., Lantenois, S., Van Aken, P.A., Bauer, A., and Plançon, A. (2012) Experimental investigation of smectite interaction with metal iron at 80ºC: structural characterization of newly formed Fe-rich phyllosilicates. *American Mineralogist*, **97**, 864–871.

Lantenois, S. (2003) Réactivié fer metal/smectites en milieu hydraté à 80ºC. PhD thesis, Université d'Orleans, Orleans, France, 220 pp.

Lantenois, S., Lanson, B., Muller, F., Bauer, A., Jullien, M., and Plançon, A. (2005) Experimental study of smectite interaction with metal Fe at low temperature: 1. Smectite destabilization. *Clays and Clay Minerals*, **53**, 597–612.

Lauretta, D.S., Hua, X., and Buseck, P.R. (2000) Mineralogy of fine-grained rims in the ALH 81002 CM chondrite. *Geochimica et Cosmochimica Acta*, **64**, 3263–3273.

Ledésert, B., Hébert, R., Grall, C., Genter, A., Dezayes, C., Bartier, D., and Gérard, A. (2009) Calcimetry as a useful tool for a better knowledge of flow pathways in the Soultz-sous-Forêts Enhanced Geothermal System. *Journal of Volcanology and Geothermal Research*, **181**, 106–114.

López García, J.A., Manteca, J.I., Prieto, A.C., and Calvo, B. (1992) Primera aparición en España de cronstedtita. Caracterización estructural. *Boletín de la Sociedad Española de Mineralogía*, **15-1**, 21–25.

McAlister, J.A. and Kettler, R.M. (2008) Metastable equilibria among dicarboxylic acids and the oxidation state during acqueous alteration on the CM2 chondrite parent body. *Geochimica et Cosmochimica Acta*, **72**, 233–241.

Miyahara, M., Uehara, S., Ohtani, E., Nagase T., Nishijima, M., Vashaei, Z., and Kitagawa, R. (2008) The anatomy of altered chondrules and FGRs covering hem in a CM chondrite by FIB-TEM-STEM. *Lunar Planetary Science*, **XXXIX**, 199–200.

Mosser-Ruck, R., Cathelineau, M., Guillaume, D., and Charpentier, D. (2010) Effects of temperature, pH, and iron/clay and liquid/clay ratios on experimental conversion of dioctahedral smectite to berthierine, chlorite, vermiculite, or saponite. *Clays and Clay Minerals*, **58**, 280–291.

Mugnaioli, E., Gorelik, T., and Kolb, U. (2009) "Ab initio" structure solution from electron diffraction data obtained by a combination of automated diffraction tomography and precession technique. *Ultramicroscopy*, **109**, 758–765.

Müller, W.F., Kurat, G., and Kracher, A. (1979) Chemical and

https://doi.org/10.1346/CCMN.2013.0610408 Published online by Cambridge University Press

crystallographic study of cronstedtite in the matrix of the Cochabamba (CM2) carbonaceous chondrite. *Tschermaks Mineralogische und Petrographische Mitteilungen*, **26**, 293–304.

Parkhurst, D.L. and Appelo, C.A.J. (1999) *User's guide to PHREEQC* (Version 2). A Computer Program for Speciation, Batch-reaction, One-dimensional Transport, and Inverse Geochemical Calculations. U.S. Geological Survey Water-Resources Investigations Report 99–4259, 312 pp.

Perronnet, M., Villiéras, F., Jullien, M., Razafitianamaharavo, A., Raynal, J., and Bonnin, D. (2007) Towards a link between the energetic heterogeneities of the edge of smectites and their stability in the context of metallic corrosion. *Geochimica et Cosmochimica Acta*, **71**, 1463–1479.

Perronnet, M., Jullien, M., Villiéras, F., Raynal, J., Bonnin, D., and Bruno, G. (2008) Evidence of a critical content in Fe(0) on FoCa7 bentonite reactivity at 80ºC. *Applied Clay Science*, **38**, 187–202.

Pierron, O. (2011) Interactions eau-fer-argilite: rôle des paramètres Liquide/Roche, Fer/Argilite, Température sur la nature des phases minérales. PhD thesis, Université Henri Poincaré, Nancy, 226 pp.

Rivard, C. (2011) Contribution à l'étude de la stabilité des minéraux constitutifs de l'argilite du Callovo-Oxfordien en présence de fer à 90ºC, PhD thesis, Institut National Polytechnique de Lorraine, Nancy, France, 338 pp.

Rivard, C., Pelletier, M., Michau, N., Razafitianamaharavo, A., Bihannic, I., Abdelmoula, M., Ghanbaja, J., and Villiéras, F. (2013) Berthierine-like mineral formation and stability during the interaction of kaolinite with metallic iron at 90ºC under anoxic and oxic conditions. *American Mineralogist*, **98**, 163–180.

Rousset, D. (2002) Etude de la fraction argileuse de séquence sédimentaires de la Meuse et du Gard. Reconstruction de l'histoire diagénetique et des caractéristiques physico-chimiques des cibles. PhD thesis, Université Louis Pasteur, Strasbourg, France, 269 pp.

Schlegel, M.L., Bataillon, C., Benhamida, K., Blanc, C., Menut, D., and Lacour, J. (2008) Metal corrosion and argillite transformation at the water-saturated, high-temperature iron-clay interface: a microscopic-scale study. *Applied Geochemistry*, **23**, 2619–2633.

Schulte, M. and Schock, E. (2004) Coupled organic synthesis and mineral alteration on the meterorite parent bodies. *Meteoritic and Planetary Science*, **39**, 1577–1590.

Smrčok, L. and Weiss, Z. (1993) DIFK91: a program for the modelling of powder diffraction patterns on a PC. *Journal of Applied Crystallography*, **26**, 140–141.

Smrčok, L., Ďurovič, S., Petříček, V., and Weiss, Z. (1994) Refinement of the crystal structure of cronstedtite-3*T*. *Clays and Clay Minerals*, **42**, 544–551.

Steadman, R. and Nuttall, P.M. (1963) Polymorphism in cronstedtite. *Acta Crystallographica*, **16**, 1–8.

Steadman, R. and Nuttall, P.M. (1964) Further polymorphism in cronstedtite. *Acta Crystallographica*, **17**, 404–406.

Sunagawa, I. (2005) *Crystals. Growth, Morphology and Perfection*. Cambridge University Press, Cambridge, UK.

Wilson, J., Cressey G., Cressey, B., Cuadros, J., Ragnarsdottir, K.V., Savage, D., and Shibata, M. (2006) The effect of iron on montmorillonite stability. (II) Experimental investigation. *Geochimica et Cosmochimica Acta*, **70**, 323–336.

Zega, T.J. and Buseck, P.R. (2003) Fine-grained-rim mineralogy of the Cold Bokkeveld CM chondrite. *Geochimica et Cosmochimica Acta*, **67**, 1711–1721.

(*Received 13 March 2013; revised 9 July 2013; AE: W. Huff; Ms. 748*)

https://doi.org/10.1346/CCMN.2013.0610408 Published online by Cambridge University Press